



HAL
open science

Multiscale NMR analysis of the degradation of apple structure due to thermal treatment

Alexandre Leca, Sylvie Clerjon, J.-M. Bonny, Catherine M. G. C. Renard,
Amidou Traoré

► To cite this version:

Alexandre Leca, Sylvie Clerjon, J.-M. Bonny, Catherine M. G. C. Renard, Amidou Traoré. Multiscale NMR analysis of the degradation of apple structure due to thermal treatment. *Journal of Food Engineering*, 2021, 294, pp.110413. 10.1016/j.jfoodeng.2020.110413 . hal-03040113

HAL Id: hal-03040113

<https://hal.inrae.fr/hal-03040113v1>

Submitted on 15 Dec 2022

HAL is a multi-disciplinary open access archive for the deposit and dissemination of scientific research documents, whether they are published or not. The documents may come from teaching and research institutions in France or abroad, or from public or private research centers.

L'archive ouverte pluridisciplinaire **HAL**, est destinée au dépôt et à la diffusion de documents scientifiques de niveau recherche, publiés ou non, émanant des établissements d'enseignement et de recherche français ou étrangers, des laboratoires publics ou privés.



Distributed under a Creative Commons Attribution - NonCommercial 4.0 International License

1 Multiscale NMR analysis of the degradation of apple structure due
2 to thermal treatment

3 Alexandre Leca^{*a}, Sylvie Clerjon^b, Jean-Marie Bonny^b, Catherine M.G.C. Renard^c,
4 Amidou Traore^b

5 ^a INRAE, Avignon Université, UMR408 SQPOV, 84914 Avignon, France

6 ^b INRAE, AgroResonance, 63122 Saint Genès Champanelle, France.

7 ^c INRAE, TRANSFORM, 44316 Nantes, France

8 ** Corresponding author: alexandre.leca@inrae.fr*

9

10 **Abstract**

11 The cooking temperature required to alter the structure of apple sticks was investigated
12 by NMR (magnetic resonance imaging (MRI) and magnetic resonance spectroscopy
13 (MRS)) to detect the thermal degradation of the vacuolar membrane, and by puncture
14 tests to detect tissue softening due to heating. Both NMR methods evidenced the pivot
15 temperature of 53 °C at which the apple parenchyma switches from “fresh” to “cooked”
16 state, i.e. loses its cellular and subcellular structuration. At the tissue scale, the puncture
17 tests performed on apple sticks also showed a shift in firmness at 53 °C. At the
18 molecular scale, the NMR measurements converged with both MRI and MRS,
19 evidencing a thermal degradation of the cell membranes leading to a change in vacuole
20 water chemical exchanges and distribution throughout the cells, cell walls and
21 intercellular spaces. These phenomena lead to a tissue homogenization with heating,
22 which is reflected by a single T_2 after cooking.

23

24 **Keywords**

25 NMR; relaxometry; puncture; thermal softening; apple; heat processing

26

27 **1. Introduction**

28

29 Understanding the response of fruit and vegetable microstructure to thermal treatment
30 is the key to assess the bioavailability of their nutrients (Parada and Aguilera, 2007), as
31 well as the texture of the fresh or processed product (Aguilera, 2005). However, because
32 of the complexity of the products involved and their multiscale properties and
33 microstructure, this relation between thermal treatment and fruit and vegetable

34 microstructure is still not completely understood. Two main mechanisms have long
35 been identified, namely loss of cellular compartmentation and cell wall degradation, the
36 later having been much more studied. However, during cooking, the first irreversible
37 reaction is the disruption of vacuolar membrane, causing a loss of cellular turgor
38 pressure and diffusion of vacuolar water (Waldron et al., 2003), which leads to a
39 softened and less structured fruit.

40 Apple is a relevant model for this study because its intrinsic microstructure and cell
41 organization have been extensively studied and are well documented (Janssen et al.,
42 2020; Khan and Vincent, 1990): apple parenchyma is structured by a network of cell
43 walls enclosing cells, mostly composed of water-rich vacuoles, and a high proportion of
44 gas-filled intercellular spaces, almost 30% of the volume in mature apples (Chiralt and
45 Fito, 2003; Mendoza et al., 2007). Most published works on apple texture concern
46 maturing and stored fresh fruits, specifically showing the impact of the cell organization
47 of apple parenchyma on the firmness and crunchiness of the fruits (Harker et al., 1997;
48 Létal et al., 2003). The porosity, *i.e.* the ratio of intercellular air space to total volume,
49 and the size of individual intercellular spaces, have been reported to contribute to apple
50 firmness and crunchiness (Harker et al., 1997; Ting et al., 2013). The impact of the
51 thermal treatment on fruit texture and quality is generally assessed through firmness
52 analysis and physicochemical analyses (de Belie et al., 2002). However, only a few
53 studies have looked at the relationship between mechanical properties and the evolution
54 of cellular structure (Kebe et al., 2015; Ng and Waldron, 1997). An efficient analytical
55 technique for monitoring microstructural changes is therefore needed.

56 Nuclear magnetic resonance (NMR) and its two modalities, nuclear magnetic resonance
57 spectroscopy (MRS) and imaging (MRI), are non-destructive and will detect objects that
58 are not modified by sample preparation. They allow to visualize and quantify the
59 heterogeneity in plant materials such as apple flesh (Winisdorffer et al., 2015), and to
60 study the evolution of fruits during storage at a high spatial resolution, revealing
61 otherwise undetectable variations (Ciampa et al., 2010).

62 More specifically, MRS is a method of choice to measure fine tissue interactions with
63 water through the proton relaxation time interaction at the sample scale, and non-
64 destructively. Gonzalez et al. (Gonzalez et al., 2010) used it on onions to study the
65 decrease in transverse relaxation time of the main water fraction with increasing
66 cooking temperature, and showed the destruction of cellular structure leading to an
67 increased exchange between water and cellular content. The evolution of the subcellular
68 structure of apple parenchyma in drying or freezing processes clearly shows that
69 changes to cell wall and cell membrane impact the transverse relaxation time (Hills and
70 Remigereau, 1997). The membranes, which are still intact, act as a barrier against water
71 exchange, and result in **a multicomponent T_2 distribution**.

72 MRI is well suited to locally quantify water concentration or how water bonds to the
73 other constituents, but at a finer spatial scale. Already in 1991, McCarthy et al
74 (McCarthy et al., 1991) followed the water content in drying apple slices using MRI. The
75 indirect measurement of T_2 and T_2^* maps, which are sensitive to discrepancies in
76 magnetic susceptibility, is used to describe the microstructure of plant tissues, while
77 preserving the sample integrity, and thus enables longitudinal study. **NMR relaxometry**
78 **methods combining MRI and MRS lets quantify (i) the relaxation time and water**

79 compartmentalization in tissues, (ii) the T_2 and permeability of cell membranes, and
80 (iii) the diffusion and magnitude of cell and intercellular transport (Van As, 2007).

81 MRI is thus a relevant approach for studying vacuolar membrane thermal degradation
82 and the subsequent diffusion of intracellular fluid filling the intercellular spaces during
83 and after thermal treatment. This method is mainly limited by its time resolution:
84 several minutes are required to produce images or spectra yielding specific parameters
85 describing the spatial distribution and mobility of water molecules, *i.e.* relaxation time
86 and diffusion coefficients. Acquisition time may be shortened either by decreasing the
87 image spatial resolution, *e.g.* as in the study of Mohoric on rice (Mohoric et al., 2009),
88 or by optimizing k-space filling, as in the study of meat cooking by Bouhrara et al.
89 (Bouhrara et al., 2012). However, existing studies focus on fresh fruits (Marigheto et al.,
90 2008; Van As and van Duynhoven, 2013) or on fruit-based model materials to
91 reproduce cellular degradation (Lahaye et al., 2018), and not on intrinsically structured
92 processed products.

93 This study addresses the hypothesis that the apple tissue thermal softening occurs as a
94 consequence of or simultaneously with the thermal degradation of the vacuolar
95 membrane, changing the tissue microstructure. To our knowledge, no study has
96 investigated the critical temperature at which the cell membranes of a fruit is highly
97 damaged. **NMR relaxometry (both imaging and spectroscopy)** was used to objectify the
98 membrane fusion temperature in the apple parenchyma on a non-processed whole fruit
99 sample. For this purpose, apple fruit samples were treated at different temperatures
100 (below and above tissular destructuration) prior to characterization by penetrometry,
101 **and NMR relaxometry. MRS relaxometry resolves multiple T_2 compartments in the**

102 whole sample, while MRI is sensitive to microstructural heterogeneities at a finer spatial
103 scale.

104 **2. Materials and methods**

105 2.1 Plant material

106 Golden Delicious apples (*Malus domestica* Borkh. var. Golden Delicious) were
107 purchased at a local supermarket (Auchan, Avignon, France) at consumable ripeness.
108 They were stored in a cold chamber at +4 °C in normal atmospheric conditions for less
109 than 8 days, and were taken out approximately 4 hours before the experiment for
110 equilibration at room temperature. For each condition, apples were cut into 12 × 8 × 30
111 mm³ sticks, the longer side being cut along the radial axis of the apple. Sticks to be
112 cooked were vacuum-sealed in food-grade plastic bags (PE-LD 30 µm, RAJA SA,
113 Tremblay-en-France, France). For the NMR measurements, six apple sticks were used
114 for each condition, each one from a different fruit. For the puncture tests, three sticks
115 were cut from both sides of an apple, except for smaller apples in which only two sticks
116 were sampled.

117 2.2 Thermal treatments

118 The thermal treatments were performed in a water bath, three apple sticks at a time.
119 The times needed to reach each cooking temperature at the center of two sticks were
120 measured in a preliminary study by inserting a thermocouple during heating; these
121 times were then used for subsequent experiments at the corresponding temperatures.
122 Consequently, the five thermal treatments were: 7 min at 45 °C, 10 min at 50 °C, 10 min
123 at 53 °C, 14 min at 60 °C and as a reference for a complete thermal denaturation, 18 min
124 at 70 °C. After thermal treatment, samples were cooled in melting ice for 8-15 minutes.

125 Samples were then kept at ambient temperature for 24 hours before measurement. This
126 24 h rest before measurement was applied because a preliminary study (*data not*
127 *shown*) had demonstrated a continuous evolution of the water status inside the apple
128 sticks occurred for 6 hours following the treatment and cooling steps.

129 2.3 Firmness measurements

130 The firmness of the samples was estimated by measuring the mean load obtained from
131 puncture tests, after preliminary tests (*data not shown*) had shown good repeatability at
132 the apple stick scale. Each sample was punctured on two faces (one along the radial axis
133 of the fruit, the other perpendicular to the radial axis), with two repetitions per face. The
134 puncture tests were done using a Ta-Plus texturometer (Lloyd Instruments Ltd., Bognor
135 Regis, UK) equipped with a 50 N load cell and a punch 2 mm in diameter and 17 mm
136 long. Penetration rate was 100 mm.min⁻¹ and puncture stopped once a 70% strain was
137 reached. Mean load at the plateau (F_{mean} , N) was determined for each test as the average
138 of 1000 data points taken from the plateau region in the force-displacement curve.

139 2.4 NMR Relaxometry

140 **Both MRI and MRS relaxometry measurements** were made on a 9.4 T Bruker
141 Ascend 400WB instrument (Bruker, Ettlingen, Germany) equipped with a
142 microimaging accessory and using a 32 mm diameter birdcage radiofrequency coil used
143 for both excitation and signal reception, at 20 °C.

144 2.4.1 MRI T_2 measurement:

145 Each of the 30 samples (raw, 45 °C, 50 °C, 53 °C and 60 °C × 6 repetitions) was placed
146 in a 25 mm tube with a reference stick (cooked for 18 min at 70 °C). Nine transversal

147 single spin echo images were acquired, intercepting both the reference and the cooked
148 sample, at nine different echo times (6.5, 8.5, 10.5, 15, 20, 40, 70, 100 and 200 ms), TR
149 = 3000 ms, voxel vol. 1 mm³ isotropic, total acquisition time 32 min. The T_2 maps were
150 built by fitting these nine echo magnitudes voxelwise, assuming mono-exponential
151 decrease. **The T_2 histogram was calculated over the six sample images, for the six**
152 **durations and temperature conditions.**

153 **For morphological analysis, high resolution MRIs were acquired in the same**
154 **experimental conditions: transversal multi-slice mono-echo image; TE/TR = 5.5/3000,**
155 **spatial resolution 0.1 × 0.1 × 0.5 mm³, field of view 1.6 × 3 cm, acquisition time 32**
156 **minutes.**

157 2.4.2 MRS T_2 measurement:

158 Spectroscopic T_2 measurements were performed using the Carr-Purcell-Meiboom-Gill
159 (CPMG) pulse sequence, $90_x^\circ - \tau - [180_y^\circ - \tau - (\text{echo})]_n$, with an interpulse delay τ of 500 μs .
160 This relatively short sampling time was used to minimize diffusion dephasing while
161 being large enough to avoid sample overheating by RF deposition. The recycle delay
162 (time to let the signal recover between successive echo acquisitions) was set to 2 s. A
163 total of $n = 256$ echoes spectra were recorded to describe the transversal echo decay
164 curve for a total acquisition time of 45 min. For each time/temperature treatment (**same**
165 **as in imaging measurements, except that the sample cooked at 70°C was measured**
166 **separately**), T_2 measurements were performed on six samples to improve robustness.

167 A common feature in biological systems is a continuous distribution of water among
168 their internal structures (Kroeker and Henkelman, 1986). Continuous water dynamic
169 distribution will therefore better reflect the biological microstructure of the apple

170 parenchyma. To estimate such continuous distribution, the measured T_2 decay curves
171 were fitted by a weighted sum of a large number m of exponentials:

$$172 \quad \mathbf{S} = \sum_{j=1}^m A_j e^{\left(-t_i/T_{2j}\right)} \quad i = 1, 2, \dots, n \quad [1]$$

173

174 Each fitting was performed with an in-house Matlab® implementation of the non-
175 negative least squares (NNLS) algorithm (Lawson and Hanson, 1995). The solution
176 given by NNLS is a sparse vector of m discrete A_j non-zero amplitudes at known T_{2j}
177 values of the given basis (Whittall and MacKay, 1989). A standard regularization
178 constraint was added to smooth the estimated discrete distribution A_j provided by
179 NNLS. The resulting distributions of T_2 relaxation times do not require defining the
180 number of exponentials beforehand, only to feed the regularized NNLS algorithm with a
181 large number of T_{2j} values (*i.e.* 200) logarithmically spaced from 1 ms to 1000 ms. The
182 regularized NNLS solution was a set of amplitudes A_j that minimizes the lack of fit:

$$183 \quad \sum_{i=1}^N \left| \sum_{j=1}^M A_{ij} S_j - y_i \right|^2 + \mu \sum_{j=1}^M |S(T_{2j})|^2, \mu \geq 0 \quad [2]$$

184 where the Lagrangian term μ is automatically calculated using the cross validation
185 approach (Whittall and MacKay, 1989).

186 To ease comparison with T_2 maps from imaging measurements, a weighted average of
187 all T_2 components was also calculated.

188

189 **3. Results**

190 3.1 Texture analysis

191 F_{mean} decreased as the heating temperature increased (Figure 1), in agreement with the
192 authors' visual and tactile observations, and the thermal softening of fruits and
193 vegetables observed in previous studies (Bourles et al., 2009; Ng and Waldron, 1997).
194 Although the value dispersion was high, especially for the apple sticks heated at 53 °C,
195 significant differences were found between three groups: {raw, 45°C, 50°C}, {53°C}, and
196 {60 °C, 70 °C}.

197 The average value of F_{mean} at 53 °C is equal to 1.16 N, which is almost halfway between
198 F_{mean} at 50 °C (1.75 N) and at 60 °C (0.5 N).

199

200 3.2 Imaging and Spectroscopy Relaxometry analyses

201 Figure 2 presents the T_2 maps obtained on six samples per temperature and duration
202 condition. Because local T_2 never exceeded 60 ms, T_2 maps were windowed from 0 to 60
203 ms. On each image, samples cooked for 18 min at 70 °C (reference final thermal
204 degradation) are presented on the left, and samples obtained with the indicated
205 treatment temperature and duration on the right.

206 **MRI relaxometry:** The distributions of T_2 within the samples calculated for each thermal
207 treatment from MRI T_2 maps are displayed in the middle part of Figure 2. For the raw
208 samples, T_2 values were very short and closely distributed around 9 ms. When the
209 treatment temperature increased, higher T_2 values appeared, mainly between 30 and 50
210 ms. For 70 °C, T_2 maps of all the reference samples (on the left in each photo in Figure
211 2) were used to obtain the T_2 distribution.

212 **MRS relaxometry:** The distribution of water proton T_2 displayed three components for
213 the six raw samples with the relative amplitudes of 70–80% for the largest T_2
214 component, 20–30% for the intermediate one and 1–5% for the lowest peak amplitude.

215 The positions of the T_2 peaks were variable, which can be attributed to the intrinsic
216 signal-to-noise ratio of the decay curve of each sample (see supplementary data, Figure
217 S3). However, considering the apple cellular structure and its compartmentalization
218 (Hills and Remigereau, 1997), the largest T_2 component (20–60 ms) can be attributed to
219 the water in vacuoles. The intermediate peak, with a T_2 value of around 100 ms, can be
220 assigned to water in cytoplasm, and the population with the shortest relaxation times
221 (around 10 ms) may be attributed to water in tight interactions with membranes and/or
222 macromolecules. The observation of three distinct relaxation times implied that the
223 diffusive exchanges between the different apple compartments were slow compared to
224 the sampling time, i.e., echo time (Belton and Ratcliffe, 1985). However, the observed T_2
225 values differed slightly from those already reported from low-field studies (Hills and
226 Remigereau, 1997). For the T_2 distribution obtained with CPMG (Figure 2, right), apple
227 heating caused a separation into two main populations (around 25 ms and 220 ms).
228 Indeed, the marked difference shown by samples subjected to 45 °C was the
229 disappearance of the lowest T_2 component. After treatment at 50 °C, samples still
230 displayed two main T_2 peaks, but the difference between their respective relaxation
231 times was small. The samples treated at 53 °C showed a distinctive pattern, with a sharp
232 separation between the T_2 pools and a marked decrease in the T_2 values (~30 ms) of the
233 largest component. After cooking at 60 °C, the two components were clearly separated,
234 with a marked decrease in the lowest component, which was shifted toward the longest
235 T_2 (100–500 ms). The sample subjected to the cooking temperature of 70 °C (the
236 reference sample) displayed one dominant component (>95%) with $T_2 = 30$ ms.
237 Thermal treatment resulted first in the reduction of the number of T_2 components (from
238 3 to 2) at lower temperature with a sharp separation observed at 53 °C. Further increase

239 in temperature led to the appearance of one dominant peak (> 95%) with a slight
240 decrease in T_2 .

241 Figure 3 shows, on the same graph, the evolution of both imaging T_2 and weighted
242 average non-resolved T_2 values versus the cooking temperature. For the fresh sample,
243 the imaging T_2 value was lower than the spatially non-resolved one, whereas these
244 values converged to nearly the same value at temperatures above 53 °C.

245 Figure 4 presents high-resolution images of raw, and 50, 53 and 60 °C treated samples.
246 The left sticks are the reference cooked (70 °C) samples. Despite the high water content
247 of apple parenchyma, MRI in Figure 4 showed a very poor signal on raw samples. Even
248 at this high spatial resolution, the presence of air-filled spaces in non- or partially-
249 cooked sample led to signal loss.

250

251 **4. Discussion**

252 Contrast in MRI of biological systems relies on the interplay of various parameters, *e.g.*
253 relaxation times, temperature, diffusion, flow and exchange, and on local differences in
254 magnetic susceptibility (Belton and Ratcliffe, 1985). MRI acquisitions were designed to
255 characterize the effect of treatment temperature on the apple parenchyma by means of
256 the T_2 relaxation maps. **The observed T_2 maps from MRI and those from MRS CPMG**
257 **results come from the interplay of various relaxation mechanisms (mainly, diffusive and**
258 **chemical exchanges) related to the experimental conditions (mainly, echo time) and**
259 **tissue characteristics (compartments size, membrane permeability, porosity, etc...). The**
260 **contribution of each relaxation mechanism, among others, to the observed T_2 have to be**
261 **taken in account in the interpretation of the results of the present study. Indeed, to**
262 **better explain the observed differences in T_2 between imaging and spectroscopy and**

263 those between raw and cooked sample, the generic expression of the observed T_2
264 relaxation was used (Edzes et al., 1998):

$$265 \quad \frac{1}{T_{2obs}} = \frac{1}{T_{2i}} + \frac{1}{T_{2exc}} + \frac{1}{T_{2g}} \quad [3]$$

266 where T_{2i} represents the intrinsic water T_2 in apple tissue, T_{2exc} represents the
267 contribution of diffusive and/or chemical exchange effects seen in both imaging and
268 spectroscopic experiments. T_{2g} comes from additional spin dephasing introduced by
269 spatial encoding gradients in imaging experiments. The latter was negligible because
270 one image acquisition per echo time was used instead of a multi-echo pulse sequence.

271 Air-filled spaces are known to account for 20 to almost 30% of the total volume of fresh
272 apple parenchyma (Chiralt and Fito, 2003; Mendoza et al., 2007). Strong local magnetic
273 field gradients (G_{loc}) originate from the differences in magnetic susceptibility at the air-
274 tissue and air-water interfaces. As a result, water diffusion through these local gradients
275 leads to an increasing contribution of T_{2exc} and consequently in a reduction of the
276 observed T_2 value. The amount of this diffusive contribution is related to G_{loc} and echo
277 time (TE) according to the expression:

$$278 \quad \frac{1}{T_{2exc}} \sim \gamma^2 G_{loc}^2 TE^2 D \quad [4]$$

279 where γ is the proton gyromagnetic ratio, and D is the diffusion coefficient of water in
280 apple tissue. Equation [4] clearly explains the predominant effect of water diffusion
281 through local field inhomogeneities on the lower signal intensity of spin echo images,
282 and the resulting lower T_2 values. Both the observed lower signal intensity in the T_2
283 weighted images of raw samples along with those cooked at temperature below 53°C
284 (Figure 4) and the lower T_2 values from T_2 maps of these samples (Figure 2) appear
285 counterintuitive given the highly mobile water located in the apple parenchyma.

286 However, this phenomenon is commonly reported in fruits or plants (Van As, 2007).
287 Even at the shortest imaging echo time (5 ms), water diffusion through apple
288 compartments is the predominant T_2 relaxation mechanism resulting also in the
289 observed single averaged T_2 , thus limiting the quantitative information about water
290 compartmentalization along with changes related to the cooking process. Decreasing TE
291 is one of the ways to minimize such diffusion effects on the measured T_2 (Equation [4]).
292 This can be achieved only with special MRI pulse sequences (Edzes et al., 1998) with
293 some constraints outside the scope of the present study. One of the simple means, as
294 used in the present study, to allow T_2 measurements with short enough TE is by non-
295 spatially resolved techniques. The CPMG measurement performed with the TE of 0.5 ms
296 yielded a distribution of T_2 relaxation time, which was in close agreement with water
297 compartmentalization in apple tissue. The observation of multiexponential components
298 also suggested that the diffusion between compartments (*i.e.* the T_{2exc} component in
299 Equation [3]) is less efficient than in imaging. **The raw apple internal membranes**
300 **(mainly the vacuolar membrane) act as a diffusion barrier (Belton and Ratcliffe, 1985)**
301 **leading to the resolution of more than one exponential decays (components).** Equation
302 [4] also indicates that the diffusion effect is mitigated at low field (G_{loc}^2 depends on the
303 field strength). This field dependency explains why our spectroscopic T_2 values were
304 smaller than those reported in the lower field studies by Hills and Duce (Hills and Duce,
305 1990) and by Hills and Remigereau (Hills and Remigereau, 1997).
306 **Figure 2 shows that the main result of increasing the cooking temperature was to**
307 **increase, from the outer to the inner, the T_2 values of the apple parenchyma, which**
308 **became either nearly homogeneous for sample cooked at 53°C or fully homogeneous for**

309 those cooked at 60°C and 70°C. Similar behavior was observed for signal intensity of
310 apple parenchyma in the high resolution T₂ weighted images (Figure 4). As stated
311 above, the lower T₂ of the raw apple parenchyma (T₂ maps) along with its lower signal
312 intensity in T₂ weighted images, regardless of high and mobile vacuolar water, are
313 related to the large amounts of air-filled spaces in the apple tissue, i.e., the susceptibility
314 effects. Consequently, the observed increase in the T₂ values in the cooked samples can
315 reasonably be attributed to a decrease or the disappearance of these air-filled spaces.
316 Furthermore, both imaging and spectroscopic T₂ results showed a marked change at
317 treatment temperature 53 °C. Consequently, we chose to analyze the cooking effect on
318 T₂ relaxation time for the two states, namely fresh *vs* cooked (before and after 53°C)
319 rather than following T₂ components as a function of treatment temperature.

320 Between 45 °C and 50 °C, thermal treatment merely induced the disappearance of the
321 low mobility water fraction, the one attributed to the water fraction in tight interaction
322 with membranes and/or macromolecules. This disappearance may be ascribed to the
323 shift toward lower relaxation time not resolved by the NNLS algorithm. This is
324 anticipated by a lower signal-to-noise ratio (SNR) of these transversal decay signals. As
325 demonstrated by Bertero and Pike (Bertero et al., 1982) and further discussed by
326 Istratov and Vyvenko (Istratov and Vyvenko, 1999), SNR in the CPMG decay curve is a
327 major factor that limits the resolution of exponential analysis. Figure 3 shows that after
328 a 45 °C and even after a 50 °C thermal treatment, the difference between the imaging T₂
329 and the averaged spatially non-resolved T₂ remained unchanged in comparison with raw
330 samples, indicating that diffusion was still dominant as the air-filled spaces were still
331 dominant. This was confirmed by the high-resolution images (Figure 4). The presence of

332 these dominant air-filled spaces along with the presence of two main T_2 components
333 suggests that the integrity of the vacuolar membrane was still preserved at 40–50 °C.
334 Beginning at 53 °C and more pronounced at 60 °C, high resolution images (Figure 4)
335 and the T_2 map (Figure 2, left) showed an increasing signal intensity in the apple
336 parenchyma. As stated above, this increase in signal intensity was associated with the
337 disappearance of the air-filled spaces, most probably owing to the internal membrane
338 leakage. The latter hypothesis was supported by the appearance of one main T_2
339 component from the spatially non-resolved CPMG analysis. As no significant changes in
340 volume of the apple sticks were observed (Figure 4), the disappearance of these air-filled
341 spaces may be due to their filling with vacuolar water after membrane leakage.
342 Goodman et al. (1996) have already reported this phenomenon in their study on
343 strawberry fruit. They attributed the reduced inhomogeneity of the local magnetic
344 susceptibility associated with the contamination of the parenchyma by *Botrytis cinerea*
345 to filling of the intercellular gas spaces with intracellular fluid released through cell wall
346 damages (Goodman et al., 1996). By 53 °C, the T_2 values from imaging maps equaled the
347 weighted average spatially non-resolved T_2 (Figure 3). This convergence is predicted by
348 Equation 4. The disappearance of air-filled spaces owing to cooking minimizes the
349 contribution of diffusion through internal field gradients in the observed T_2 . The latter
350 becomes almost independent in TE used in imaging and spectroscopy CPMG (Figure 3).
351 However, these T_2 values (30–40 ms) remained smaller than those reported from lower
352 field studies and with lower TE (Hills & Duce, 1990). These differences can this time be
353 attributed to chemical exchanges between water protons and exchangeable protons
354 belonging to macromolecules, *e.g.* polysaccharides. This phenomenon is well
355 documented in the literature and the reader will find a characteristic description for the

356 apple in the work of Hills and Duce (Hills & Duce, 1990). In short, in the absence of
357 diffusion within internal magnetic field susceptibility, at long TE, the additional
358 dephasing due to chemical exchanges in the observed T_2 (*i.e.* T_{2exc} in Equation [3])
359 becomes effective and more pronounced at high magnetic field strengths with the
360 increased difference in the chemical shifts between the exchangeable sites, namely water
361 protons and protons belonging to macromolecular exchangeable sites.

362 The relevance of considering two states (uncooked under 53 °C and cooked from 53 °C)
363 rather than each thermal treatment separately, as evidenced by the NMR study, is
364 confirmed by the texture analysis, the F_{mean} results being divided into three groups :
365 under 53 °C (uncooked), 53 °C (transitional temperature), above 53 °C (cooked).

366 This resistance to heat up to 50 °C is in line with previous findings (Kim et al., 1993). To
367 our knowledge, no study has been performed on moderately high temperatures: existing
368 studies are either at temperatures below 50°C or above 90 °C (Bourles et al., 2009), nor
369 on the transitional temperature at which apple parenchyma softens.

370 However, existing studies focusing on fruit thermal treatment show the release of
371 vacuolar water due to the thermal degradation of the vacuolar membrane and other
372 cellular membranes as the first cause of apple tissue thermal degradation (Kunzek et al.,
373 1999). This is followed by complex and non-comprehensively documented hydrolysis
374 mechanisms occurring within the cell wall and inducing further thermal softening,
375 especially at high temperatures (Christiaens et al., 2016; Van Buren, 1979), added to a
376 potential degradation of the water sorption capacity of the cell wall during or after
377 thermal treatment (Kebe et al., 2015; Le Bourvellec et al., 2011). **The endogenous**
378 **enzymes, especially the pectin methylesterase (PME), can also modify the**
379 **microstructure (Kunzek et al., 1999). Apple PME has low activity at the natural pH of**

380 apple (Denes et al., 2000) and it is stable in apple below 60 °C (El-Shamei et al., 2008),
381 although once purified its activity rapidly decreases when heated above 52 °C (Denès et
382 al., 2000). Endogeneous enzymes modify the cell wall resulting in two contrasted
383 consequences: the joint action of PME and polygalacturonase leads to cell wall
384 degradation (Sams et al., 1993), but the PME activity on its own may lead to consecutive
385 demethylated galacturonic sequences that form gels with calcium and strengthen the
386 cell walls (Barry-Ryan, 2012; Waldron et al., 2003). These enzymatic modifications of
387 the cell wall could be increased by the thermal degradation of the vacuolar membrane,
388 facilitating the access to cell wall for the PME.

389 The cooked apples sticks had a gel-like aspect, with a glassy appearance, whereas the
390 uncooked sticks were opaque. This observation results of the air substitution with
391 vacuolar water and is in agreement with spectroscopic studies on degraded fruit tissue
392 (Valero et al., 2004; Zerbini et al., 2002). During sample preparation, cutting a raw stick
393 produced qualitatively more juice than cutting a cooked stick. Such change would lead
394 to the compartmentization and distribution of the cellular content within the whole
395 tissue, at temperatures higher than or equal to 53 °C. This in turn results in a cloudiness
396 and an enhanced fluid retention in the cell wall, expressed in the MRS results as a
397 decreased T_2 .

398

399 **5. Conclusion**

400 NMR T_2 relaxometry was used to examine Golden Delicious apple fruit microstructure
401 after thermal treatment. **Both MRI and MRS relaxometry** detected the thermal damage
402 of cell membrane resulting in the leakage of vacuolar water and the filling of
403 intercellular spaces, revealed by a clear shift in T_2 patterns at the pivot temperature of

404 53 °C. The parallel firmness analysis evidenced to determine that the softening of apple
405 parenchyma occurred simultaneously at 53 °C. Thus there was no detectable delay
406 between the molecular and the tissue response of apple to thermal treatment, enabling a
407 direct control of cooking and its impact on firmness and the chemical exchanges within
408 the tissue. Although all *Malus domestica* cultivars have the same microstructural
409 properties, differences in chemical composition of the vacuole, turgor pressure in cell,
410 composition of the cell wall, are likely to impact the cell membrane resistance to thermal
411 treatment, therefore the pivot temperature between raw and cooked. Thus this work
412 only confirms 53 °C as the cooking temperature for Golden Delicious cultivar.
413 This multiscale study also confirms that **NMR T₂ relaxometry** allows to explain the
414 microstructural impact of thermal treatment, and to detect the transition temperature
415 between raw and cooked, which correlates with texture loss.

416

417 **Acknowledgements**

418 All NMR experiments were performed at the AgroResonance Platform, INRAE (DOI
419 10.15454/1.5572398324758228e12). This work was funded by INRAE TRANSFORM
420 Research Department.

421

422 **CRedit authorship contribution statement**

423 **Alexandre Leca:** Conceptualization; Methodology; Investigation; Supervision; Writing
424 – original draft. **Sylvie Clerjon:** Investigation; Methodology; Writing – original draft.

425 **Jean-Marie Bonny:** Supervision; Writing – review & editing. **Catherine MGC**

426 **Renard:** Supervision; Writing – review & editing. **Amidou Traore:** Investigation;

427 Methodology; Writing – original draft.

428 **References**

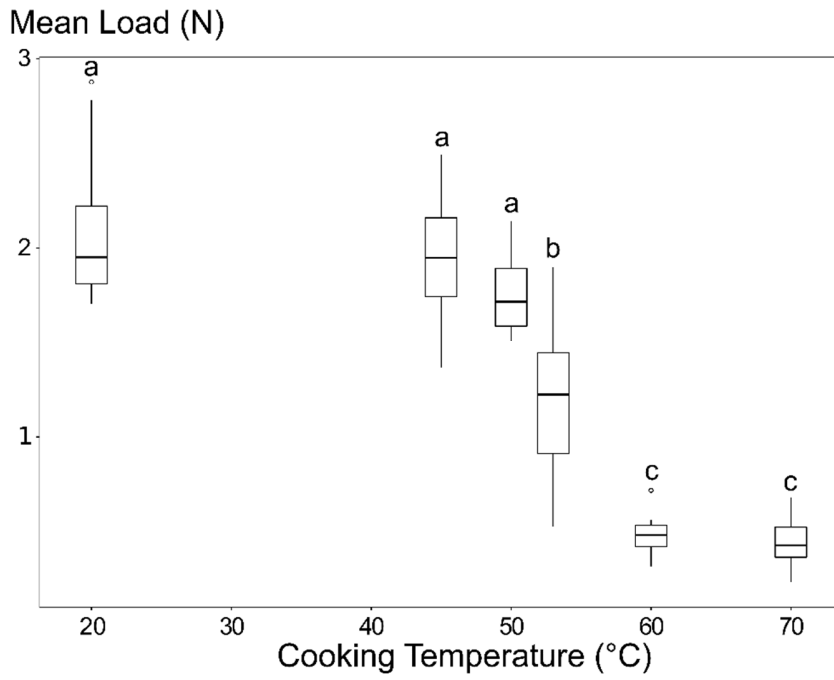
- 429 Aguilera, J.M., 2005. Why food microstructure? *Journal of Food Engineering* 67, 3–11.
 430 <https://doi.org/10.1016/j.jfoodeng.2004.05.050>
- 431 Belton, P.S., Ratcliffe, R.G., 1985. NMR and compartmentation in biological tissues.
 432 *Progress in Nuclear Magnetic Resonance Spectroscopy* 17, 241–279.
 433 [https://doi.org/10.1016/0079-6565\(85\)80010-8](https://doi.org/10.1016/0079-6565(85)80010-8)
- 434 Bertero, M., Boccacci, P., Pike, E.R., 1982. On the recovery and resolution of exponential
 435 relaxation rates from experimental data: a singular-value analysis of the Laplace
 436 transform inversion in the presence of noise. *Proceedings of the Royal Society of*
 437 *London. A. Mathematical and Physical Sciences* 383, 15–29.
 438 <https://doi.org/10.1098/rspa.1982.0117>
- 439 Bouhrara, M., Clerjon, S., Damez, J.-L., Kondjoyan, A., Bonny, J.-M., 2012. In Situ
 440 Imaging Highlights Local Structural Changes during Heating: The Case of Meat.
 441 *J. Agric. Food Chem.* 60, 4678–4687. <https://doi.org/10.1021/jf2046569>
- 442 Bourles, E., Mehinagic, E., Courthaudon, J.L., Jourjon, F., 2009. Impact of vacuum
 443 cooking process on the texture degradation of selected apple cultivars. *Journal of*
 444 *Food Science* 74, E512–E518. <https://doi.org/10.1111/j.1750-3841.2009.01360.x>
- 445 Chiralt, A., Fito, P., 2003. Transport Mechanisms in Osmotic Dehydration: The Role of
 446 the Structure: *Food Science and Technology International* 9, 179–186.
 447 <https://doi.org/10.1177/1082013203034757>
- 448 Christiaens, S., Van Buggenhout, S., Houben, K., Jamsazzadeh Kermani, Z., Moelants,
 449 K.R.N., Ngoumazong, E.D., Van Loey, A., Hendrickx, M.E.G., 2016. Process-
 450 Structure-Function Relations of Pectin in Food. *Crit Rev Food Sci Nutr* 56, 1021–
 451 1042. <https://doi.org/10.1080/10408398.2012.753029>
- 452 Ciampa, A., Dell’Abate, M.T., Masetti, O., Valentini, M., Sequi, P., 2010. Seasonal
 453 chemical–physical changes of PGI Pachino cherry tomatoes detected by magnetic
 454 resonance imaging (MRI). *Food Chemistry* 122, 1253–1260.
 455 <https://doi.org/10.1016/j.foodchem.2010.03.078>
- 456 de Belie, N., Laustsen, A.M., Martens, M., Bro, R., Baerdemaeker, J.D., 2002. Use of
 457 Physico-Chemical Methods for Assessment of Sensory Changes in Carrot Texture
 458 and Sweetness During Cooking. *Journal of Texture Studies* 33, 367–388.
 459 <https://doi.org/10.1111/j.1745-4603.2002.tb01354.x>
- 460 Edzes, H.T., van Dusschoten, D., Van As, H., 1998. Quantitative T2 imaging of plant
 461 tissues by means of multi-echo MRI microscopy. *Magn Reson Imaging* 16, 185–
 462 196. [https://doi.org/10.1016/S0730-725X\(97\)00274-9](https://doi.org/10.1016/S0730-725X(97)00274-9)
- 463 Gonzalez, M.E., Barrett, D.M., McCarthy, M.J., Vergeldt, F.J., Gerkema, E., Matser,
 464 A.M., Van As, H., 2010. (1)H-NMR study of the impact of high pressure and
 465 thermal processing on cell membrane integrity of onions. *Journal of food science*
 466 75, E417–25. <https://doi.org/10.1111/j.1750-3841.2010.01766.x>
- 467 Goodman, B.A., Williamson, B., Simpson, E.J., Chudek, J.A., Hunter, G., Prior, D.A.M.,
 468 1996. High field NMR microscopic imaging of cultivated strawberry fruit.
 469 *Magnetic Resonance Imaging* 14, 187–196. [https://doi.org/10.1016/0730-725X\(95\)02051-T](https://doi.org/10.1016/0730-725X(95)02051-T)
- 470
 471 Harker, F.R., Redgwell, R.J., Hallett, I.C., Murray, S.H., Carter, G., 1997. Texture of
 472 Fresh Fruit, in: *Horticultural Reviews*. John Wiley & Sons, Ltd, pp. 121–224.
 473 <https://doi.org/10.1002/9780470650646.ch2>

474 Hills, B.P., Duce, S.L., 1990. The influence of chemical and diffusive exchange on water
475 proton transverse relaxation in plant tissues. *Magnetic Resonance Imaging* 8,
476 321–331. [https://doi.org/10.1016/0730-725X\(90\)90106-C](https://doi.org/10.1016/0730-725X(90)90106-C)
477 Hills, B.P., Remigereau, B., 1997. NMR studies of changes in subcellular water
478 compartmentation in parenchyma apple tissue during drying and freezing.
479 *International Journal of Food Science and Technology* 32, 51–61.
480 <https://doi.org/10.1046/j.1365-2621.1997.00381.x>
481 Istratov, A.A., Vyvenko, O.F., 1999. Exponential analysis in physical phenomena.
482 *Review of Scientific Instruments* 70, 1233–1257.
483 <https://doi.org/10.1063/1.1149581>
484 Janssen, S., Verboven, P., Nugraha, B., Wang, Z., Boone, M., Josipovic, I., Nicolai, B.M.,
485 2020. 3D pore structure analysis of intact ‘Braeburn’ apples using X-ray micro-
486 CT. *Postharvest Biology and Technology* 159, 111014.
487 <https://doi.org/10.1016/j.postharvbio.2019.111014>
488 Kebe, M., Renard, C.M.C.G., El Maâtaoui, M., Amani, G.N.G., Maingonnat, J.-F., 2015.
489 Leaching of polyphenols from apple parenchyma tissue as influenced by thermal
490 treatments. *Journal of Food Engineering* 166, 237–246.
491 <https://doi.org/10.1016/j.jfoodeng.2015.05.037>
492 Khan, A.A., Vincent, J.F.V., 1990. Anisotropy of apple parenchyma. *Journal of the*
493 *Science of Food and Agriculture* 52, 455–466.
494 <https://doi.org/10.1002/jsfa.2740520404>
495 Kim, D.M., Smith, N.L., Lee, C.Y., 1993. Apple Cultivar Variations in Response to Heat
496 Treatment and Minimal Processing. *Journal of Food Science* 58, 1111–1114.
497 <https://doi.org/10.1111/j.1365-2621.1993.tb06126.x>
498 Kroeker, R.M., Henkelman, M.R., 1986. Analysis of biological NMR relaxation data with
499 continuous distributions of relaxation times. *Journal of Magnetic Resonance*
500 (1969) 69, 218–235. [https://doi.org/10.1016/0022-2364\(86\)90074-0](https://doi.org/10.1016/0022-2364(86)90074-0)
501 Kunzek, H., Kabbert, R., Gloyna, D., 1999. Aspects of material science in food
502 processing: changes in plant cell walls of fruits and vegetables. *Z Lebensm Unters*
503 *Forsch* 208, 233–250. <https://doi.org/10.1007/s002170050410>
504 Lahaye, M., Bouin, C., Barbacci, A., Le Gall, S., Foucat, L., 2018. Water and cell wall
505 contributions to apple mechanical properties. *Food Chem* 268, 386–394.
506 <https://doi.org/10.1016/j.foodchem.2018.06.110>
507 Lawson, C.L., Hanson, R.J., 1995. Solving Least Squares Problems, *Classics in Applied*
508 *Mathematics*. Society for Industrial and Applied Mathematics.
509 <https://doi.org/10.1137/1.9781611971217>
510 Le Bourvellec, C., Bouzerzour, K., Ginies, C., Regis, S., Plé, Y., Renard, C.M.G.C., 2011.
511 Phenolic and polysaccharidic composition of applesauce is close to that of apple
512 flesh. *Journal of Food Composition and Analysis*, 8th International Food Data
513 Conference: Quality food composition data, key for health and trade 24, 537–547.
514 <https://doi.org/10.1016/j.jfca.2010.12.012>
515 Létal, J., Jiráček, D., Šuderlová, L., Hájek, M., 2003. MRI ‘texture’ analysis of MR images
516 of apples during ripening and storage. *LWT - Food Science and Technology* 36,
517 719–727. [https://doi.org/10.1016/S0023-6438\(03\)00099-9](https://doi.org/10.1016/S0023-6438(03)00099-9)
518 Marigheto, N., Venturi, L., Hills, B., 2008. Two-dimensional NMR relaxation studies of
519 apple quality. *Postharvest Biology and Technology* 48, 331–340.
520 <https://doi.org/10.1016/j.postharvbio.2007.11.002>

- 521 McCarthy, M.J., Perez, E., Özilgen, M., 1991. Model for Transient Moisture Profiles of a
522 Drying Apple Slab Using the Data Obtained with Magnetic Resonance Imaging.
523 *Biotechnology Progress* 7, 540–543. <https://doi.org/10.1021/bp00012a009>
- 524 Mendoza, F., Verboven, P., Mebatsion, H.K., Kerckhofs, G., Wevers, M., Nicolai, B.,
525 2007. Three-dimensional pore space quantification of apple tissue using X-ray
526 computed microtomography. *Planta* 226, 559–570.
527 <https://doi.org/10.1007/s00425-007-0504-4>
- 528 Mohoric, A., Vergeldt, F., Gerkema, E., van Dalen, G., van den Doel, L.R., van Vliet, L.J.,
529 Van As, H., Van Duynhoven, J., 2009. The effect of rice kernel microstructure on
530 cooking behaviour: A combined mu-CT and MRI study. *Food Chem.* 115, 1491–
531 1499. <https://doi.org/10.1016/j.foodchem.2009.01.089>
- 532 Ng, A., Waldron, K.W., 1997. Effect of Cooking and Pre-Cooking on Cell-Wall Chemistry
533 in Relation to Firmness of Carrot Tissues. *Journal of the Science of Food and*
534 *Agriculture* 73, 503–512. [https://doi.org/10.1002/\(SICI\)1097-
535 0010\(199704\)73:4<503::AID-JSFA762>3.0.CO;2-Z](https://doi.org/10.1002/(SICI)1097-0010(199704)73:4<503::AID-JSFA762>3.0.CO;2-Z)
- 536 Parada, J., Aguilera, J. m., 2007. Food Microstructure Affects the Bioavailability of
537 Several Nutrients. *Journal of Food Science* 72, R21–R32.
538 <https://doi.org/10.1111/j.1750-3841.2007.00274.x>
- 539 Ting, V.J.L., Silcock, P., Bremer, P.J., Biasioli, F., 2013. X-Ray Micro-Computer
540 Tomographic Method to Visualize the Microstructure of Different Apple
541 Cultivars. *Journal of Food Science* 78, E1735–E1742.
542 <https://doi.org/10.1111/1750-3841.12290>
- 543 Valero, C., Ruiz-Altisent, M., Cubeddu, R., Pifferi, A., Taroni, P., Torricelli, A., Valentini,
544 G., Johnson, D., Dover, C., 2004. Selection Models for the Internal Quality of
545 Fruit, based on Time Domain Laser Reflectance Spectroscopy. *Biosystems*
546 *Engineering* 88, 313–323. <https://doi.org/10.1016/j.biosystemseng.2004.03.012>
- 547 Van As, H., 2007. Intact plant MRI for the study of cell water relations, membrane
548 permeability, cell-to-cell and long distance water transport. *J. Exp. Bot.* 58, 743–
549 756. <https://doi.org/10.1093/jxb/erl157>
- 550 Van As, H., van Duynhoven, J., 2013. MRI of plants and foods. *J. Magn. Reson.* 229,
551 25–34. <https://doi.org/10.1016/j.jmr.2012.12.019>
- 552 Van Buren, J.P., 1979. The Chemistry of Texture in Fruits and Vegetables. *Journal of*
553 *Texture Studies* 10, 1–23. <https://doi.org/10.1111/j.1745-4603.1979.tb01305.x>
- 554 Waldron, K.W., Parker, M. l., Smith, A.C., 2003. Plant Cell Walls and Food Quality.
555 *Comprehensive Reviews in Food Science and Food Safety* 2, 128–146.
556 <https://doi.org/10.1111/j.1541-4337.2003.tb00019.x>
- 557 Whittall, K.P., MacKay, A.L., 1989. Quantitative interpretation of NMR relaxation data.
558 *Journal of Magnetic Resonance* (1969) 84, 134–152.
559 [https://doi.org/10.1016/0022-2364\(89\)90011-5](https://doi.org/10.1016/0022-2364(89)90011-5)
- 560 Winisdorffer, G., Musse, M., Quellec, S., Devaux, M.F., Lahaye, M., Mariette, F., 2015.
561 MRI investigation of subcellular water compartmentalization and gas
562 distribution in apples. *Magn. Reson. Imaging* 33, 671–680.
563 <https://doi.org/10.1016/j.mri.2015.02.014>
- 564 Zerbini, P.E., Grassi, M., Cubeddu, R., Pifferi, A., Torricelli, A., 2002. Nondestructive
565 detection of brown heart in pears by time-resolved reflectance spectroscopy.
566 *Postharvest Biology and Technology* 25, 87–97. [https://doi.org/10.1016/S0925-
567 5214\(01\)00150-8](https://doi.org/10.1016/S0925-5214(01)00150-8)

568 **Figures**

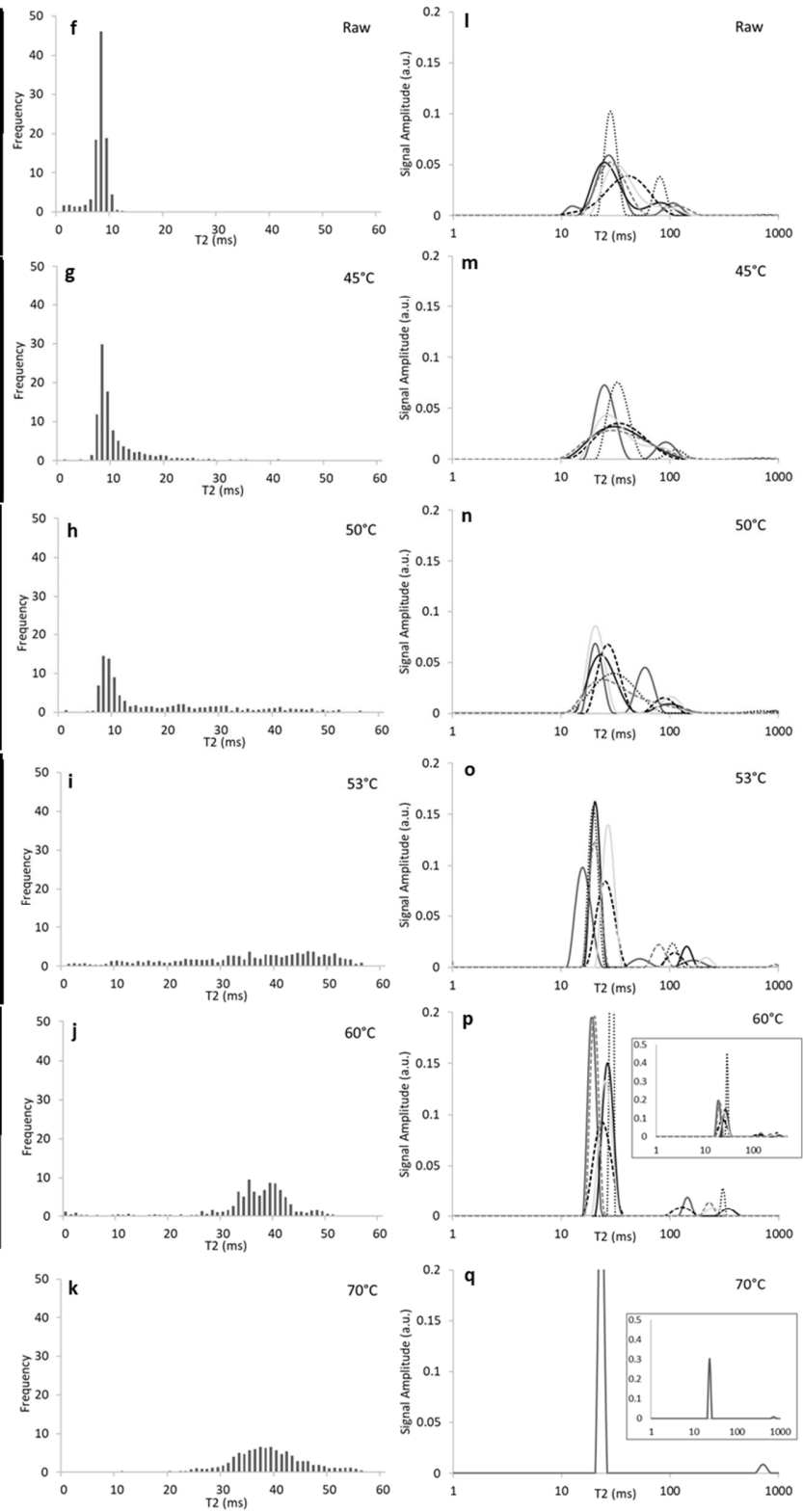
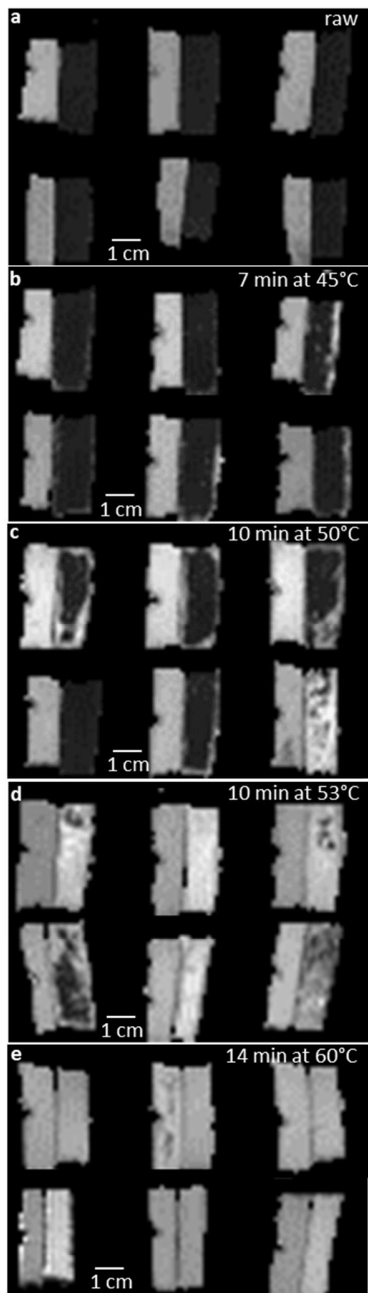
569



570

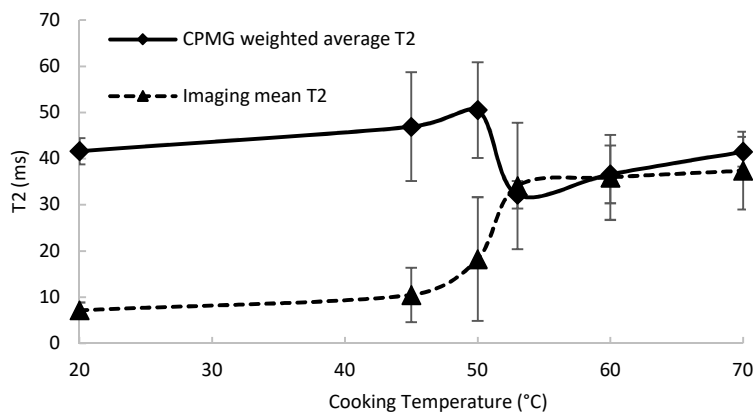
571 Figure 1: Mean Load (F_{mean}) obtained by puncture tests on the apple sticks heated at the studied
572 cooking temperatures (24 points per temperature, 20°C is the raw stick)

573



575 Figure 2: T_2 maps windowed from 0 to 60 ms (left) for raw (a), 45 °C (b), 50 °C (c), 53 °C (d) and
 576 60 °C (e) thermal treatment. The six samples are displayed for each thermal treatment. For each
 577 sample, the treated sample (on the right) is placed against a reference sample (on the left)
 578 cooked for 18 min at 70 °C. Distribution of T_2 within the samples (middle) for raw (f), 45 °C (g),
 579 50 °C (h), 53 °C (i), 60 °C (j) and 70 °C (k). T_2 distribution, obtained with CPMG, for the 6
 580 samples at raw (l), 45 (m), 50 (n), 53 (o), 60 (p) and 70 °C (q).

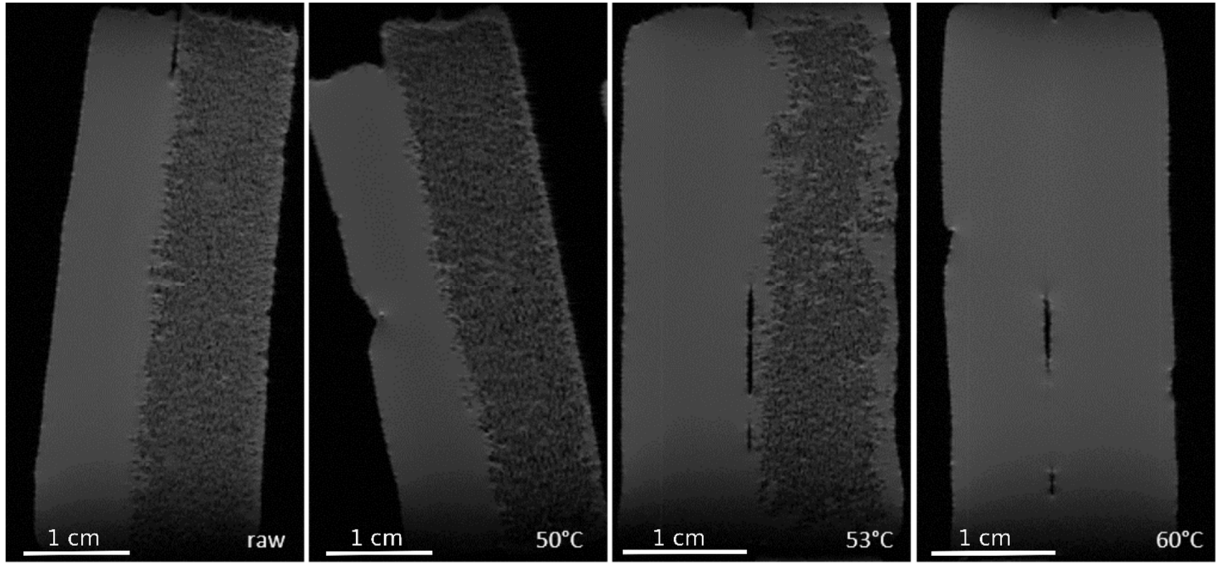
581
 582



583

584 Figure 3: T_2 variation with cooking temperature. 20°C means raw sample. Solid line: PMG
 585 average T_2 . This average is weighted by the population of each T_2 value. Dotted line: imaging T_2
 586 averaged over the whole images of samples cooked at a given cooking temperature.

587
 588



589

590 Figure 4: High-resolution MRI images of raw, and 50, 53 and 60 °C treated samples. The left
591 sticks are the reference cooked (70 °C) samples.

592

593

594

595